Journal Pre-proofs

Modulating solvated structure of Zn^{2+} and inducing surface crystallography by a simple organic molecule with abundant polar functional groups to synergistically stabilize zinc metal anodes for long-life aqueous zinc-ion batteries

Xiaoqin Zhang, Yujun Zhai, Bin Xie, Min Li, Haoran Lang, Yi Yang, Ji Chen, Yuxiang Chen, Qiaoji Zheng, Yu Huo, Ruyi Zhao, Kwok-Ho Lam, Dunmin Lin

Please cite this article as: X. Zhang, Y. Zhai, B. Xie, M. Li, H. Lang, Y. Yang, J. Chen, Y. Chen, Q. Zheng, Y. Huo, R. Zhao, K-H. Lam, D. Lin, Modulating solvated structure of Zn^{2+} and inducing surface crystallography by a simple organic molecule with abundant polar functional groups to synergistically stabilize zinc metal anodes for long-life aqueous zinc-ion batteries, *Journal of Colloid and Interface Science* (2024), doi: https://doi.org/10.1016/j.jcis.2024.05.014

Modulating Solvated Structure of Zn^{2+} and Inducing Surface Crystallography by a Simple Organic Molecule with Abundant Polar Functional Groups to Synergistically Stabilize Zinc Metal Anodes for Long-life Aqueous Zinc-ion Batteries

Xiaoqin Zhang[1], Yujun Zhai[1], Bin Xie[1], Min Li[1], Haoran Lang[1], Yi Yang[1], Ji Chen[1], Yuxiang Chen[1], Qiaoji Zheng[1], Yu Huo[1], Ruyi Zhao[2.3]*, Kwok-Ho Lam[4,]*, Dunmin Lin[1],*

[1]College of Chemistry and Materials Science, Sichuan Normal University, Chengdu 610066, China

[2]School of Energy Science and Engineering, Harbin Institute of Technology, Harbin 150001, P. R. China

[3]Shanghai Electro-Mechanical Engineering Institute, Shanghai 201109, P. R. China

[4]Centre for Medical and Industrial Ultrasonics, James Watt School of Engineering, University of Glasgow, Glasgow, Scotland, U.K.

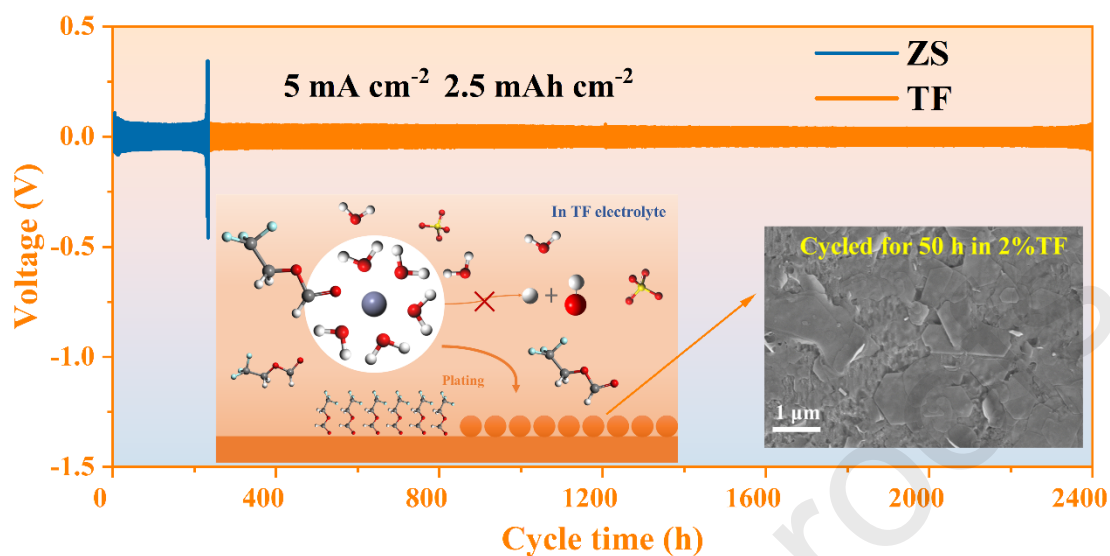## Table of contents entry

[1]Corresponding authors: E-mail addresses: 20S102159@stu.hit.edu.cn (Ruyi Zhao); kwokho.lam@glasgow.ac.uk (Kwok-Ho Lam); Fax: +86 28 84760802 Tel: +86 2884760802; ddmd222@sicnu.edu.cn (Dunmin Lin)

22 Chen, Qiaoji Zheng, Yu Huo, Ruyi Zhao, Kwok-ho Lam, Dunmin Lin

23

24 2,2,2-trifluronate (TF) infiltrates into the solvated sheath of hydrated Zn^{2+} and adheres

25 to the surface of Zn anode, guiding the homogeneous deposition of Zn^{2+} along the

26 Zn(002) crystal surface, significantly inhibiting the formation of Zn dendrites and

27 mitigrating side reactions.

28

29

Abstract

31 Aqueous zinc-ion batteries (AZIBs) have attracted significant attention owing to

32 their inherent security, low cost, abundant zinc (Zn) resources and high energy density.

33 Nevertheless, the growth of zinc dendrites and side reactions on the surface of Zn

34 anodes during repeatedly plating/stripping shorten the cycle life of AZIBs. Herein, a

35 simple organic molecule with abundant polar functional groups, 2,2,2-trifluoroether

36 formate (TF), has been proposed as a high-efficient additive in the $ZnSO_4$ electrolyte

37 to suppress the growth of Zn dendrites and side reaction during cycling. It is found that

38 TF molecules can infiltrate the solvated sheath layer of the hydrated Zn^{2+} to reduce the

39 number of highly chemically active H_2O molecules owing to their strong binding

40 energy with Zn^{2+}. Simultaneously, TF molecules can preferentially adsorb onto the Zn

41 surface, guiding the uniform deposition of Zn^{2+} along the crystalline surface of Zn(002).

42 This dual action significantly inhibits the formation of Zn dendrites and side reactions,

43 thus greatly extending the cycling life of the batteries. Accordingly, the Zn//Cu

44 asymmetric cell with 2 % TF exhibits stable cycling for more than 3,800 cycles,

45 achieving an excellent average Columbic efficiency (CE) of 99.81 % at 2 mA cm^{-2}/1

46 mAh cm^{-2}. Meanwhile, the Zn||Zn symmetric cell with 2 % TF demonstrates a

47 superlong cycle life exceeding 3,800 hours and 2,400 hours at 2 mA cm^{-2}/1 mAh cm^{-2}

48 and 5 mA cm^{-2}/2.5 mAh cm^{-2}, respectively. Simultaneously, the Zn//VO$_2$ full cell with

49 2 % TF possesses high initial capacity (276.8 mAh g^{-1}) and capacity retention (72.5 %)

50 at 5 A g^{-1} after 500 cycles. This investigation provides new insights into stabilizing Zn

51 metal anodes for AZIBs through the co-regulation of Zn^{2+} solvated structure and

52 surface crystallography.

53 Keywords: Aqueous zinc-ion batteries; Electrolyte additive; Side reaction; Zinc

54 dendrites

55

56

1. Introduction

58 As environmental pollution and the depletion of fossil fuel reserves compel us to

3

59 pursue greener and alternative energy solutions, the need to cultivate safe and reliable

60 renewable energy sources is imperative[1-4]. Electric energy is convenient and

61 environmentally friendly[5-7]. Nevertheless, due to the limited availability of Li

62 resources and the concerns regarding the security of commonly used organic

63 electrolytes in lithium-ion batteries, there is a compelling need to develop new aqueous-

64 based rechargeable batteries[8, 9]. As one of potential candidates, aqueous zinc-ion

65 batteries (AZIBs) using zinc (Zn) metal as anodes are promising due to their low

66 oxidation-reduction potential, large mass energy density (820 mAh g^{-1}) and

67 environmental friendliness[10-12]. Nevertheless, Zn anodes currently encounter with

68 rampant dendrite growth and severe side reactions involving hydrogen evolution and

69 corroding reactions. These issues shorten the lifespan and hinder the practicality of the

70 batteries[13-16]. Therefore, the development of dendrite-free Zn metal anodes for long-

71 life AZIBs is essential.

72 Recently, many strategies have been proposed to suppress the dendrite growth and

73 side reactions during Zn plating/stripping, including the construction of protective

74 layers, microstructural design of Zn anodes, and electrolyte additives[17, 18]. Among

75 them, the incorporation of additives into Zn salt aqueous electrolytes has been

76 considered as a highly convenient and efficient strategy to promote the reversibility of

77 Zn metallic anodes in AZIBs. This is achieved by regulating the primary solvation shell

78 and/or deposition behavior of Zn ions, which is valued for its simplicity, universality,

79 and cost-effectiveness[19-26]. For example, Wu et al. added 10% N, N-

80 dimethylacetamide (DMA) in ZnSO$_4$ electrolyte and found that DMA has higher

81 binding energy and stronger solvation with Zn^{2+} than H_2O, thus regulating Zn^{2+}

82 solvation shell and extending the life of the Zn‖Zn-symmetric battery to be more than

83 700 h at a current density of 0.5 mA cm^{-2}[27]. Luo et al. introduced a small amount of

84 pyridine (Py) into zinc sulfate aqueous electrolyte, adjusting the solvation shell of the

85 of Zn^{2+}, inhibiting water decomposition and therefore enabling long cycling of over

86 3,000 h at a particular current density level of 0.5 mA cm^{-2}[28]. Li et al. reshaped the

87 structure of the Zn^{2+}-solvated shell and stabilized the hydrogen bond network within

88 the bulk electrolyte using propylene glycol (PG) additives, offering optimal cycle

89 stability for full PG-protected batteries[29]. In addition, formamide, diethylene glycol

90 monoethyl ether and methyl acetate can be used to extend the cycle life of AZIBs[30-

91 32]. To our knowledge, 2,2,2-trifluoroether formate (TF) possesses abundant polar

92 functional classes such as C-O and C=O bonds, which may offer a much stronger

93 binding force with Zn^{2+} compared to H_2O. Thus, it is expected to be a high-efficiency

94 electrolyte additive for AZIBs.

95 Herein, a simple organic molecule of TF with abundant polar functional groups is

96 proposed as an additive to the electrolyte for inhibiting Zn dendrites and adverse

97 reactions while plating/stripping for AZIBs. It has been found that TF molecules can

98 enter the solvation sheath of Zn^{2+} to replace part of highly chemically active H_2O

99 molecules due to their strong binding energy with Zn^{2+} ions. Simultaneously, these

100 molecules can regulate crystallization behavior of Zn^{2+} because TF can preferentially

101 adsorb on the surface of Zn and guide the uniform deposition of Zn^{2+}. This leads to a

102 significant suppression of Zn dendrite formation and side reactions during

103 electrochemical reactions. Accordingly, with using the 2 % TF electrolytes, the

104 asymmetric Zn||Cu cell is capable of cycling stably for over 3,800 cycles at 2 mA cm^{-2}

105 ^{2}/1 mAh cm^{-2}, giving an outstanding median Columbic efficiency (CE) of 99.81 %,

106 while the Zn||Zn cell possesses the excellent cycle life of 3,800 hours at 2 mA cm^{-2}/1

107 mAh cm^{-2}.

108

2. Experimental

110 (1) Preparation of electrolytes

111 Zinc sulfate (ZnSO$_4$·7H$_2$O, Cologne, 99 %) was dissolved in deionized water (DI

112 water) to obtain a 2 M ZnSO$_4$ baseline electrolyte (ZS). TF (HCO$_2$CH$_2$CF$_3$, Macklin,

113 98 %) with different concentrations (1 %, 2 %, 3 %) was added to 2 M ZnSO$_4$

114 electrolyte to obtain TF-containing electrolytes. The optimal concentration of TF was

115 2 %.

116

117 (2) Preparation of electrodes

118 The purchased Zn foil (Qinghe Haoxuan metal material Co., LTD, thicknesses:100

119 μm, 99.99 %) was polished to remove the oxidation layer, and then cut into discs (φ =

120 10 mm) to be used as Zn electrodes.

121 VO$_2$ nanosheets were prepared by a hydrothermal method. 2 mmol of ammonium

122 metavanadate (Aladdin, 99.5 %) was dissolved in 15 mL of DI water under magnetic

123 stirring, and then 3 mmol of oxalic acid (Aladdin, 99 %) solution was added and stirred

124 for 30 min. The obtained mixture was transferred to a 100 mL autoclave lined with

125 PTFE and kept at 180 °C for 24 hours. Subsequently, the synthesized powders were

126 washed several times with ethanol (Cologne, 99.7 %) and DI water and dried in a

127 vacuum oven for 1 day to obtain VO_2 powder. The positive electrode was prepared by

128 mixing VO_2 powders, acetylene black and polyvinylidene fluoride (PVDF) (Aladdin,

129 99 %) in a mass ratio of 7:2:1 with 1-Methyl-2-pyrrolidinone (NMP, Macklin, 99 %)

130 as solvent. The slurry was then casted on a Ti foil. After dried in vacuum at 70 °C

131 overnight, the electrode with VO_2 was obtained (cathode loading: 1 mg/cm^2).

132 (3) Material characterizations and electrochemical properties

133 X-ray diffraction (XRD) analysis of samples was characterized by the XRD

134 equipment (Smart Lab, Rigaku, Japan) with a Cu-Kα (λ = 1.540598 Å, Smart Lab)

135 source (scan rate: 2 min^{-1}) and 2θ ranging from 10° to 80°. The morphology of samples

136 was studied by field emission scanning electron microscopy (SEM, FEI, Sirion 200).

137 The elemental analysis of samples was carried out using field emission scanning

138 electron microscopy (SEM, FEI-Quanta 250, USA) with energy dispersive x-ray (EDX)

139 elemental mapping.

140 All tested CR2032-type coin cells were assembled in air, and the amount of

141 electrolyte used in the coin cells was 200 μL. The VO_2//Zn full cell was assembled with

142 the Zn foil (thickness: 100 μm) as the anode and VO_2 as the cathode. The cyclic

143 voltammetry (CV) was tested in the electrolytic cell with a Ti plate as the working

144 electrode, Pt plate as the reverse electrode, and Ag/AgCl as the reference electrode.

145 With using Zn plate as the working electrode, Pt plate as the reverse electrode and

146 Ag/AgCl as the reference electrode, the linear scanning voltametric (LSV) curves and

7

147 Tafel diagrams were measured with the electrolytic cell. The chronoamperometry (CA)

148 was obtained by Amperometric *i-t* Curve testing with Zn plate as the working electrode,

149 Pt plate as the reverse electrode, and Zn plate as the reference electrode at a voltage of

150 -150 mV. The electrochemical impedance spectroscopy (EIS) of cells were conducted

151 in a frequency range of 100 kHz to 1 Hz. The above tests were performed on an

152 electrochemical workstation (CHI760E, CHI660E, Shanghai, China). With using Zn

153 plate as anode, 20 μm-thick Cu foil as cathode and glass fiber as diaphragm, a Zn-Cu

154 half battery was assembled, and its CE test was carried out on the Land CT5001A

155 battery test device.

156 A home-made optical Zn||Zn battery was designed for *in situ* observation of Zn

157 deposition in different electrolytes. The transparent Zn||Zn cell consists of a Zn plate

158 and a glass dish. The Zn plate was fixed to the bottom of the glass dish before adding

159 the electrolyte, ensuring full immersion of the Zn plate in the solution. The transparent

160 Zn||Zn cell was tested for Zn stripping/plating using a cell tester (LAND, China) at a

161 current density of 20 mA cm^{-2}, in which a video camera (NSZ-808) was used to observe

162 and record the growth of Zn dendrites.

163

164 (4) MD Simulations

165 The simulations for the structures of $ZnSO_4$ electrolyte systems with and without TF

166 were performed using the forcite module in Materials Studio. The information of

167 Lennard Jones (LJ) potential parameters was taken from the condensed-phased

168 optimized molecular potential for the atomistic simulation studies force field. The

169   Restrained ElectroStatic Potential (RESP) is the most reliable method to calculate the

170   charge. Multiwfn software was used to calculate the RESP charge of the system[33].

171   One system is composed of 18 Zn^{2+} ions, 18 SO_4^{2+} ions, and 2,000 H_2O molecules,

172   while the other contains extra 9 TF molecules. Moreover, a potential cutoff radius of

173   1.85 nm was applied for the calculation of non-bonded interactions, with electrostatic

174   interactions represented at the atomic level. Each system was then equilibrated under

175   the constant-pressure–constant-temperature (NPT) ensemble at a constant temperature

176   of 298 K to attain an equilibrium state with zero pressure for 4,000 ps. For analysis, the

177   properties of solvated structures were received in the last 1 ns. The radial distribution

178   functions (RDFs) were calculated using the analysis tool in Materials Studio.

179

180   (5) Density functional theory (DFT) calculation

181   The study of the component interactions and the solvation structures in two

182   electrolyte systems was calculated by the Gaussian16 software package. The structural

183   optimization and energy calculation were performed at M06-2X density functional and

184   def2-TZVP basis set. The Solute Electron Density (SMD) implicit solvation model was

185   used to describe the solvation effect. The electrostatic potential (ESP) was obtained

186   from Multiwfn and VMD software package. We performed ESP analysis on the vdW

187   surface with an electron density of 0.001 au (0.63 kcal/mol)[34, 35].

188   The calculations of interaction between Zn metal and electrolyte components were

189   performed by the ORCA package using a cluster model. A 6×5 supercell with a three-

190   layer Zn slab (002) was used to represent the absorbed surface for molecules, while the

191   boundary atoms were fixed to maintain the bondage of the real physical environment.

192   The structural optimization was performed at PBE0-D3(BJ)/def2-SV(P) level.

193   Considering the impact of Basis Set Superposition Error (BSSE) on the results, we

194   adopted a more accurate def2-QZVP basis set when calculating single-point energy.

195   The adsorption energy between Zn metal substrate and different electrolyte components

196   was defined as the following equation:

197   $E_{ad} = E_{total} - E_{Zn} - E_{H_2O/TF}$

198   where E_{total}, E_{Zn}, and $E_{H_2O/TF}$ are energies of the whole system, the Zn metal

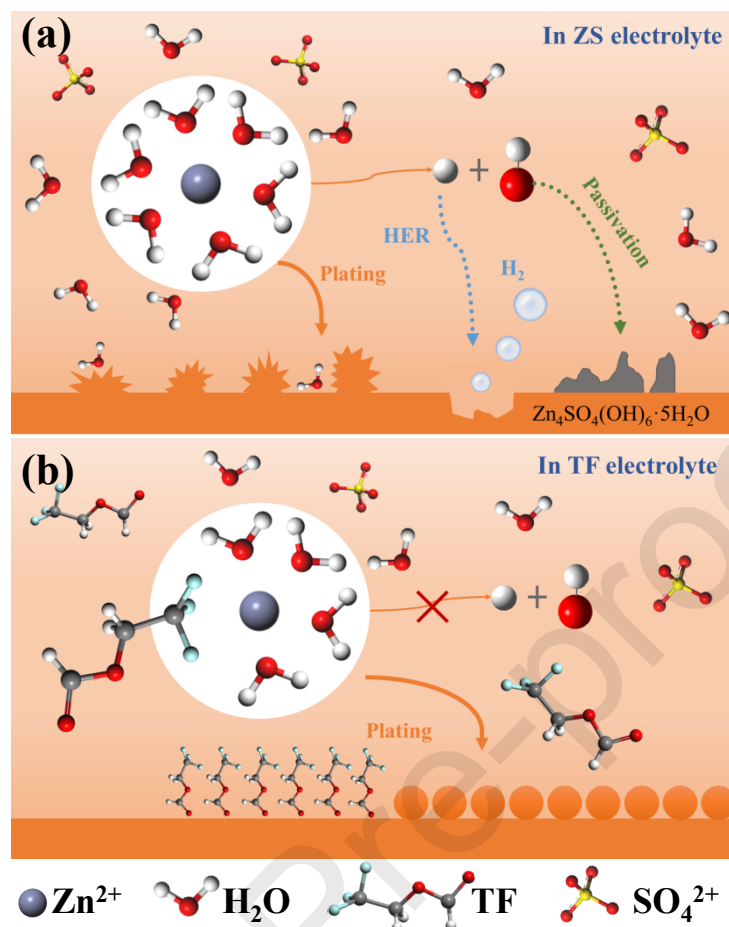199   substrate, and the H_2O molecule or TF, respectively.

200

201   (6) Calculation of the cumulative plating capacity

202   Cumulative plating capacity = Current density $\times$ Total Zn plating time

203

204   **3. Results and Discussion**

Fig. 1 Scheme representations of Zn^{2+} deposition in ZS electrolyte without and with 2 % TF.

All the experimental details are presented in the Supplementary Information. As shown in Fig.1a, in the $ZnSO_4$ (ZS) electrolyte, there are six water molecules around Zn^{2+}, forming a hydrated Zn ion, denoted as $[Zn(H_2O)_6]^{2+}$. When the hydrated Zn ions approach the Zn metal anode surface, they release six high chemical activity H_2O, which readily reduce to H_2. The process increases the local pH value and forms the co-product of $Zn_4SO_4(OH)_6 \cdot xH_2O$ (ZSH). The unevenness of the Zn anode surface is aggravated by the numerous by-products, resulting in uneven distribution of electric field, and eventually generating extensive Zn dendrites that puncture the separation and

216   cause the battery failure quickly. In contrast, in the 2 % TF electrolytes, some of the

217   H_2O in the Zn^{2+} solvated structure is replaced by TF, forming a new solvated structure.

218   The reduction in the amount of chemically active H_2O helps preventing hydrogen

219   evolution and corrosion. Simultaneously, the uniform Zn^{2+} deposition is induced along

220   the crystalline surface of Zn(002) because the TF molecules can preferentially adsorb

221   on the surface of Zn and guide the uniform Zn^{2+} deposition, which significantly inhibits

222   Zn dendrite growth and side reactions and extend battery cycle life. It is obvious that

223   the Zn metal anode with TF exhibits strong resistance against side reactions and the

224   ability to homogenize the electric fields during deposition, effectively prolonging the

225   cycle life of the battery.

226
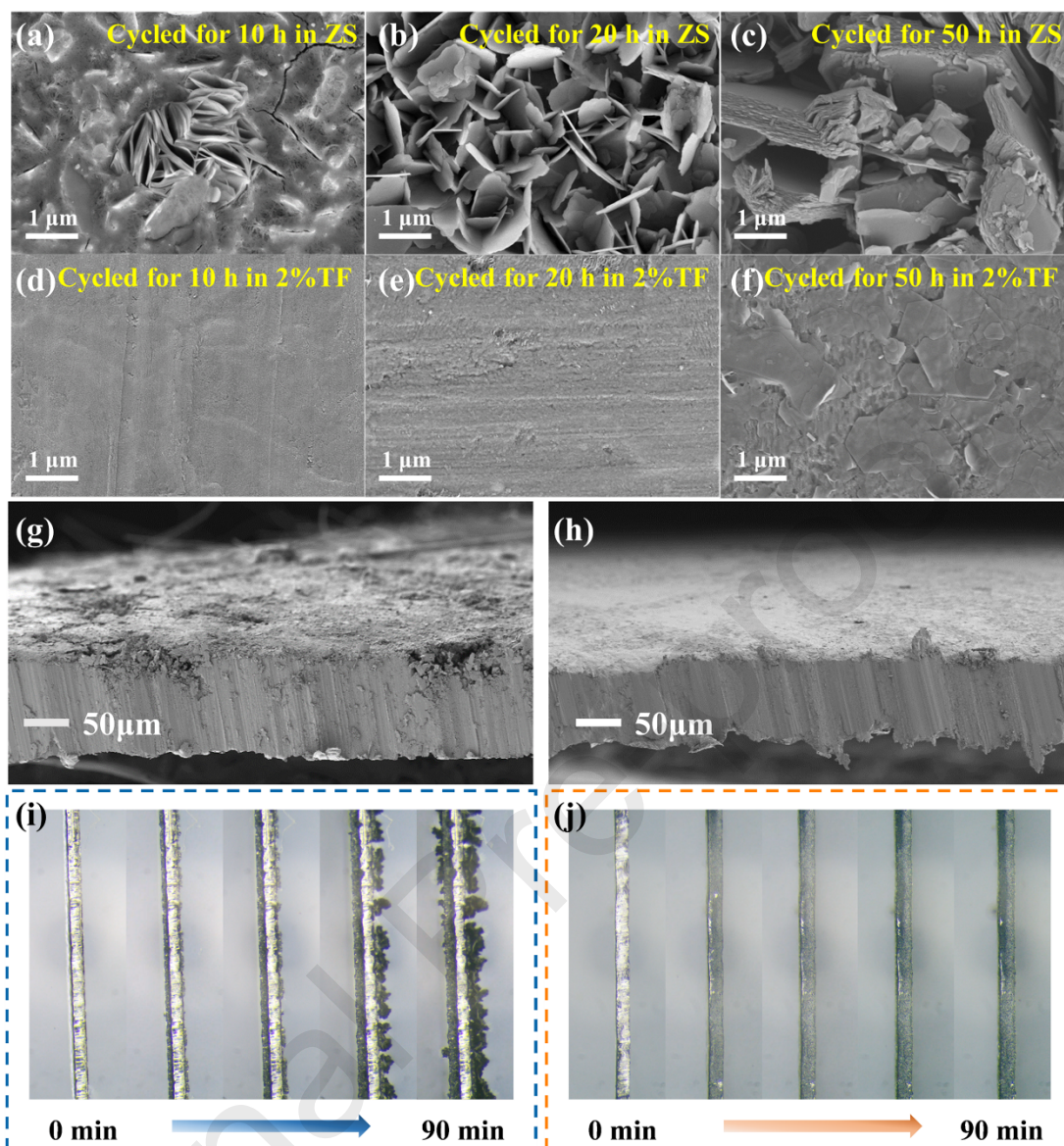
Fig. 2 SEM images of surface of Zn anode cycled for 10, 20 and 50 hours in (a – c) ZS

and (d – f) 2 % TF electrolytes. SEM images of cross section of Zn anode cycled for 50

hours in (g) ZS and (h) 2 % TF electrolytes. *In situ* optical photos of galvanizing in (i)

ZS and (j) 2 % TF electrolytes for 90 minutes.

To check the corrosion resistance of the TF additive, Zn foils are soaked in ZS

electrolytes without/with 2 % TF for 5 days, as shown in Fig. S1 (Supplementary

Information). In Fig. S1a, many sharp nanosheets are vertically/obliquely grown on the

Zn foil surface soaked in the ZS electrolyte, and the surface is loose and porous,

235 indicating serious corrosion. On the other hand, the Zn sheet impregnated with the 2 %

236 TF electrolyte exhibits a relatively smooth and dense surface without apparent

237 protuberances, suggesting that TF effectively inhibits the corrosive reactions, thereby

238 significantly reducing the formation of by-products. After immersed the Zn foil in the

239 electrolyte without TF, as shown in Fig. S2, obvious characteristic peaks of by-product

240 ZSH (PDF#39-0688) appear on the Zn foil surface, but no obvious characteristic peaks

241 of by-product are detected on the surface of Zn foil soaked in the 2 % TF electrolyte.

242 To verify the effect of the TF on the inhibition of Zn dendrite growth, the Zn||Zn-

243 symmetric batteries assembled with different electrolyte solutions are cycled for 10, 20

244 and 50 hours at 1 mA cm^{-2}/1 mAh cm^{-2}, respectively, as shown in Figs. 2a-f. The surface

245 morphologies of the Zn anodes are observed by SEM. For the Zn foil cycled in the ZS

246 electrolyte for 10 hours, obvious dendrites perpendicular to the Zn foil surface are

247 observed. As the cycle time extends, dendrites proliferate with the increasing size.

248 Consequently, the surface becomes very rough with more by-products and voids, as

249 shown in Figs. 2a – c, g. On the contrary, as shown in Figs. 2d – f, h and S3, the surface

250 of Zn foil is still very smooth and flat without an obvious dendritic structure after cycled

251 in the 2 % TF electrolyte for 10 – 50 hours, which is similar to the surface and cross-

252 section micromorphology of the original Zn foil. Similarly, the distributions of

253 elements in Figs. S4 and S5 show that large amounts of O and S elements are detected

254 on the Zn foil surface after cycled in the ZS electrolyte for 50 hours, whereas no

255 appreciable O and S elements are found in the Zn foil cycled in the 2 % TF electrolyte

256 for 50 hours. In addition, obvious characteristic peaks of by-product ZSH are detected

257   on the Zn foil surface cycled in the 2 % TF electrolyte for 5 hours; in contrast, no by-

258   product is detected on the surface of the Zn foil cycled in the ZS electrolyte (Fig. S6).

259   In addition, to study the orientation anisotropy, the crystal structures of deposited Zn

260   obtained from different electrolytes are further characterized by XRD. For the Zn metal,

261   the (002) crystal plane exhibits a smoother and much uniform interfacial charge density

262   than the (100) plane[36], thus the smooth deposition of Zn ions is facilitated by a high

263   XRD $I_{(002)}/I_{(100)}$ peak intensity ratio. The $I_{(002)}/I_{(100)}$ value of the original Zn foil is 2.44,

264   as shown in Fig. S7, but the values are changed to 0.94 and 4.08 after cycled in the ZS

265   and 2 % TF electrolytes, respectively, for 50 hours. This suggests that the Zn ion

266   deposition mainly occurs along the (002) crystal planes, but the TF molecules modify

267   the preferential direction of Zn plating, resulting in homogeneous deposition in the

268   horizontal plane (Figs. S8, S9). Density functional theory (DFT) calculations are used

269   to compare the adsorption capacities of H_2O, TF, and Zn(002). The adsorption energies

270   of water and TF molecules on the surface of Zn(002) are found to be -13.5 kcal mol^{-1}

271   and -87.2 kcal mol^{-1}, respectively, indicating that the TF molecules are more

272   preferentially adsorbed on the surfaces of Zn(002) than H_2O. This results in the

273   homogeneous precipitation of Zn^{2+} and inhibits the growth of dendrites.

274   The electrochemical deposition behaviour of Zn^{2+} is observed *in situ* by optical

275   microscopy in different $ZnSO_4$ electrolytes at 10 mA cm^{-2}, as shown in Figs. 2i, j and

276   Videos S1, S2, to intuitively assess the inhibitory effect of the additive on Zn dendrites.

277   In the ZS electrolyte, the Zn foil surface gradually becomes rough, displaying large and

278   small bumps. As the plating time increases, the Zn foil surface becomes even more

279   uneven, and the deposited Zn appears loose and porous, as shown in Fig. 2i and Video

280   S1. However, as shown in Fig. 2j and Video S2, in the 2 % TF electrolyte, as time goes

281   on, the Zn foil surface remains compact and flat without noticeable bulges. In addition,

282   the uniform deposition of Zn^{2+} is also evident from the side view, as shown in Fig. S10.

283   The conclusion that can be drawn is that the addition of additive TF effectively inhibits

284   the growth of dendrites and promotes the deposition of Zn^{2+} into a compact Zn layer,

285   rather than a loose and porous one. Furthermore, after the addition of TF to the $ZnSO_4$

286   solutions, the contact angle between the electrolytes and the Zn foils decreases,

287   indicating improved wettability of the electrolytes, as shown in Fig. S11. This improved

288   wetting capability facilitates the reversible plating/stripping at the electrode/electrolyte

289   interface.
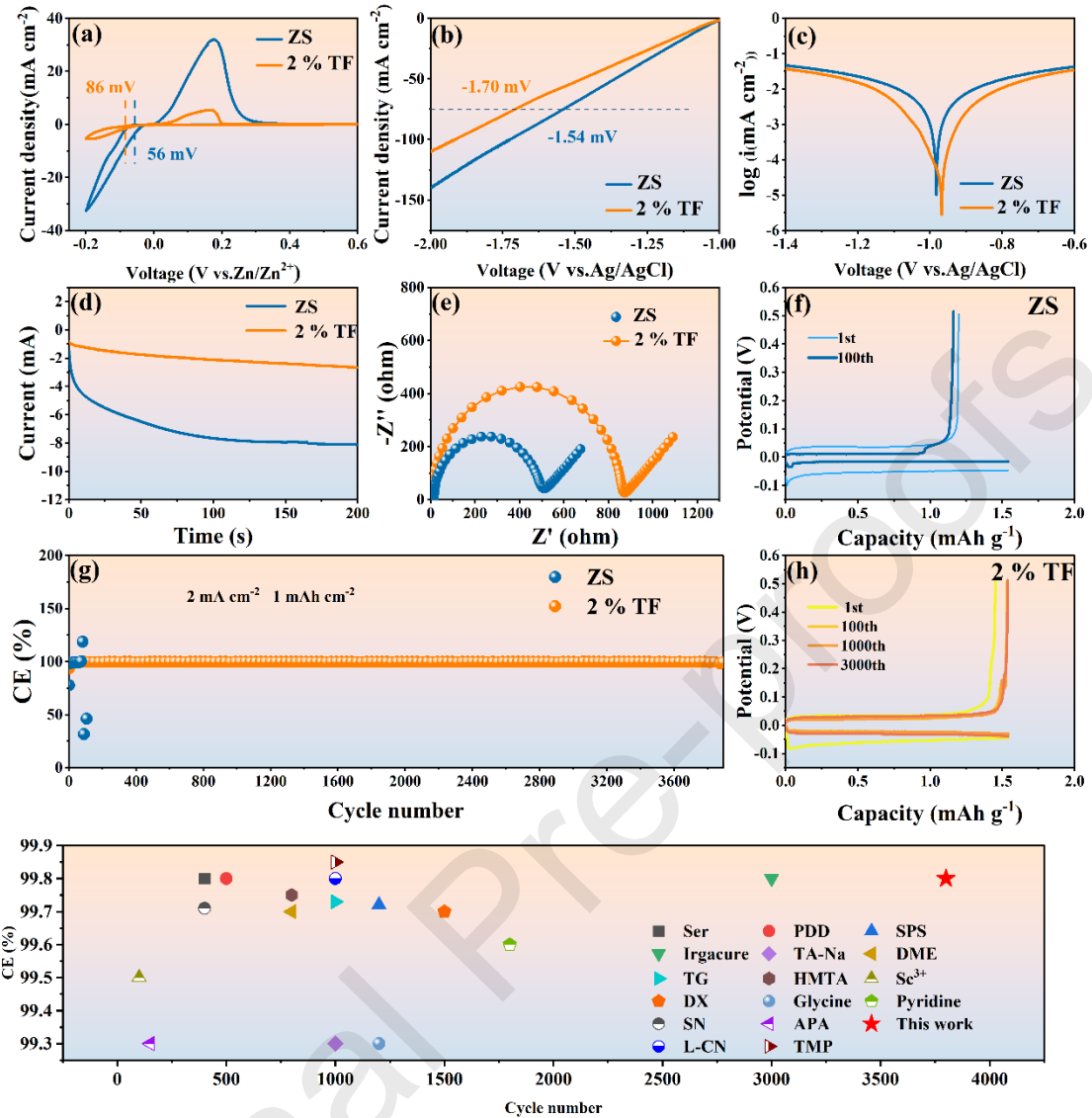
Fig. 3 (a) CV profiles of Zn foil in ZS and 2 % TF electrolytes at 1 mV s^{-1}. (b) LSV responses of Zn metals in ZS and 2 % TF electrolytes at 5 mV s^{-1}. (c) Tafel plots of Zn foil in ZS and 2 % TF electrolytes at 5 mV s^{-1} based on a three-electrode system. (d) Chronoamperometry curves of the Zn^{2+} deposition process in ZS and 2 % TF electrolytes. (e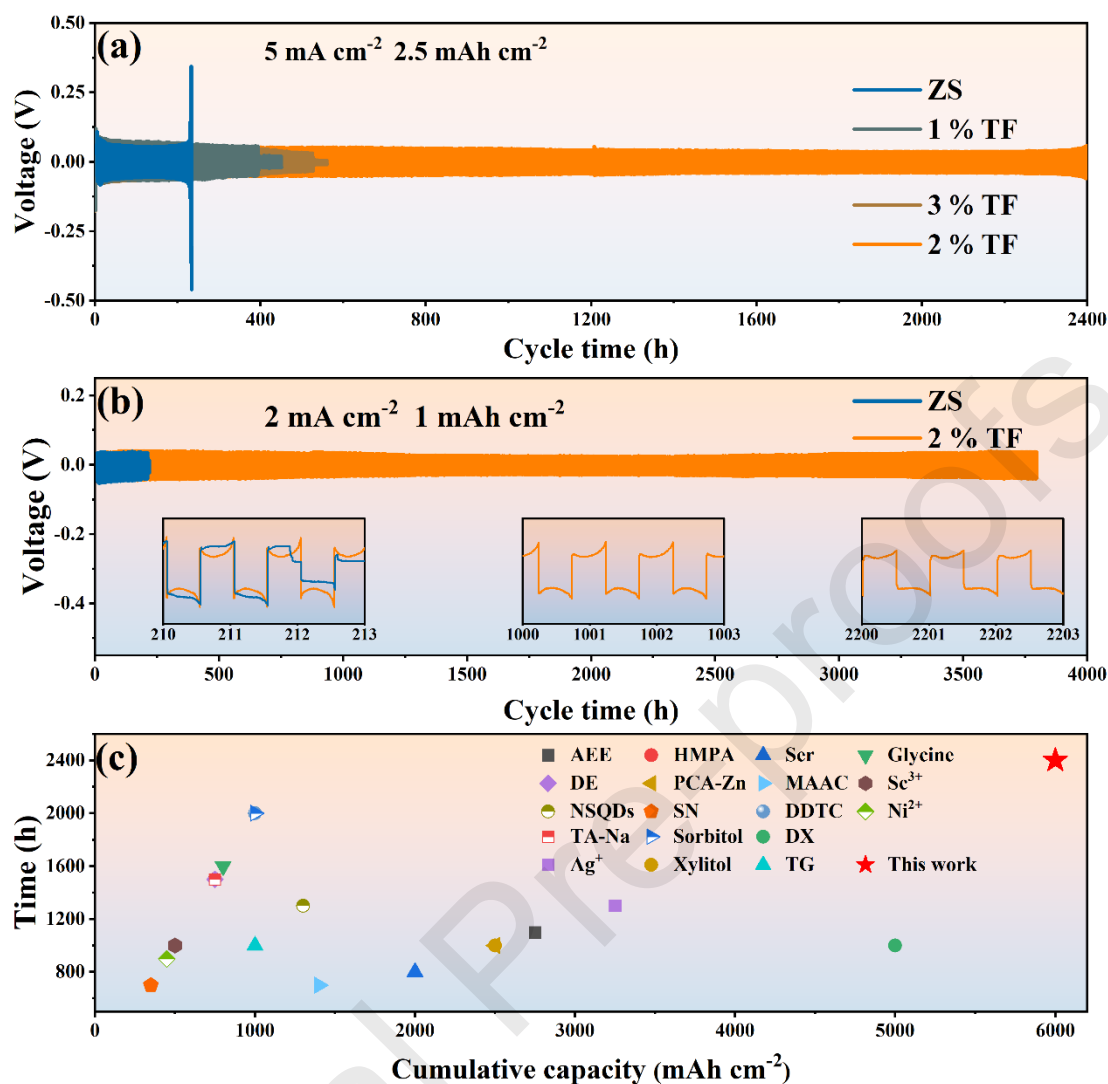) EIS spectra of Zn∥Zn symmetric cells in ZS and 2 % TF electrolytes. (f – h) Coulombic efficiency of asymmetric Zn∥Cu cells in ZS and 2 % TF electrolytes. (i) Comparison of reported values of mean CE and cycle number of Zn∥Cu half cells with this work[19, 37-52].

17

299   Cyclic voltammetry (CV) is used to study the effects of TF on the nucleation of Zn

300   ions (Fig. 3a). Clearly, the inclusion of TF enhances the nucleation over-potential of

301   Zn^{2+}, inhibiting the aggregation of Zn^{2+} into dendrites. The linear scanning voltametric

302   (LSV) curves of the Zn metals in the ZS and 2 % TF electrolytes are shown in Fig. 3b.

303   The potential of the Zn foil in the ZS electrolyte for the hydrogen-extraction reaction

304   (HER) is -1.55 V (relative to Ag/AgCl), which is significantly greater than that (-1.71

305   mV) in the 2 % TF electrolyte, at a current density of 75 mA cm^{-2}, indicating that the

306   HER is effectively suppressed after the addition of TF. The Tafel test is used to verify

307   the effect of TF on inhibiting Zn metals from corrosion. In Fig. 3c, after the addition of

308   2 % TF, the corrosion potential shows a significant increase, suggesting that the

309   presence of TF can effectively suppress the corrosion reaction. This observation aligns

310   with the XRD results shown in Fig. S2. Chronoamperometry (CA) curves (Fig. 3d) are

311   used to further investigate the mechanism underlying the distinct deposition behaviors

312   of Zn^{2+} in various electrolytes. At a constant overpotential, the current in the ZS

313   electrolyte steadily increases over 200 seconds, indicating a rapid two-dimensional (2D)

314   diffusion process with a swiftly escalating current, facilitating the dendrite growth.

315   Conversely, in the 2 % TF electrolyte, the current experiences a slow rise following an

316   initial increase. This suggests a limited 2D distribution process, aiding in the inhibition

317   of Zn dendritic growth and promoting the deposition of dense and flat Zn. The

318   electrochemical impedance spectroscopy (EIS) spectra of Zn||Zn-symmetric cells in the

319   ZS electrolyte and 2 % TF electrolyte are shown in Fig. 3e. After the introduction of

320   TF, the impedance of the symmetric cell significantly increases, which indicates that

321 the addition of TF reduces the conductivity of the electrolyte (Fig. S12). Additionally,

322 the temperature-dependence EIS is used to evaluate the desolvation capability of the

323 electrical double layer (EDL) at the interface. Figs. S13a and b show the EIS spectra of

324 the Zn‖Zn symmetric cell in ZS and 2 % TF electrolytes from 30 to 70 °C, while the

325 corresponding activation energies (E_a) derived from the Arrhenius equation are

326 presented in Figs. S13c and d. Furthermore, the addition of TF leads to an increase in

327 the Zn^{2+} transfer number $t_{Zn^{2+}}$ from 0.63 to 0.91 (Fig. S14). The smaller E_a value of Zn

328 electrode and the larger $t_{Zn^{2+}}$ in 2 % TF electrolyte (28.37 kJ mol^{-1}, 0.91) compared to

329 those in the pristine ZS electrolyte (36.32 kJ mol^{-1}, 0.63) verify the facilitated Zn^{2+}

330 interfacial desolvation and transfer during plating/stripping processes. Zn‖Cu

331 asymmetric batteries is assembled to evaluate the Coulombic efficiency (CE) of Zn

332 electrodes, as shown in Figs. 3f – h. With an initial CE of 77.79 % and failure after 111

333 hours, the battery with ZS electrolyte cycles erratically. Nevertheless, the cell with 2 %

334 TF electrolyte starts with a high CE of 93.81 %, maintaining an outstanding average

335 CE of 99.81% over 3,800 cycles, as shown in Figs. 3f – h. As shown in Fig. 3i and

336 Table S1[19, 37-52], when compared to other recently reported advanced electrolyte

337 additive systems, asymmetric Zn//Cu batteries incorporating 2 % TF demonstrate

338 comparable or even superior CE and cycle life.

339

Fig. 4 (a) Long-term cyclic behaviors of Zn‖Zn-symmetric cells in ZS electrolytes with

different TF concentrations at 5 mA cm^{-2}/2.5 mAh cm^{-2}. (b) Long-term cycling

behavior of Zn‖Zn-symmetric batteries in ZS and 2 % TF electrolytes at 2 mA cm^{-2}/1

mAh cm^{-2}. (c) Comparison of cumulative plating capacity and cycle number of Zn‖Zn

half cells with 2 % TF electrolyte with other recently reported Zn‖Zn half-cell data[38,

40, 42, 44-47, 49, 53-60].

To evaluate the effect of TF on the electrochemical cycle stability and rate

performance, Zn‖Zn-symmetric batteries are assembled with different concentrations

of TF as shown in Figs. 4a, b and S15. The Zn‖Zn-symmetric cells are cycled in the ZS

349   electrolytes with 0 %, 1 %, 2 % and 3 % TF at 5 mA cm^{-2}/2.5 mAh cm^{-2} to determine

350   the optimal TF concentration. In Fig. 4a, the cycle life of the cell with 2 % TF electrolyte

351   is over 2,400 hours, which is much longer than those of the cells with 0 % (230 hours),

352   1 % (396 hours) and 3 % (526 hours), thus, the optimal concentration of TF is 2 % for

353   the Zn anode stabilization. Fig. S15 shows the rate performance of the Zn||Zn-

354   symmetric battery at current densities from 1 to 10 mA cm^{-2}. When cycled in the ZS

355   electrolyte, the cycle life of cell does not exceed 60 hours. In contrast, the Zn||Zn

356   balanced battery demonstrates stable cyclic voltage even after 140 hours when cycled

357   in the 2 % TF electrolyte, indicating significantly improved rate performance. At 2 mA

358   cm^{-2}/1 mAh cm^{-2}, the symmetrical batteries with the 2 % TF electrolyte have a cycle

359   life of 3,800 hours that is much longer than the cell cycled in the ZS electrolyte (212

360   hours), as shown in Fig. 4b. The initial nucleation overpotentials at different current

361   currents are shown in Fig. S16. Regardless of the current density of 2 mA cm^{-2} or 5 mA

362   cm^{-2}, the nucleation overpotentials with additives are consistently lower than those

363   observed in ZS electrolyte. This suggests that the addition of 2 % TF in the electrolyte

364   enhances the migration number, which is consistent with the above test results. Both

365   Fig. 4c and Table S2 show that the addition of TF effectively prolongs the Zn||Zn-

366   symmetric battery cycle life, showing comparable or even superior cycle life and

367   cumulative capacity to recently reported work on electrolyte additives[38, 40, 42, 44-

368   47, 49, 53-60].

369
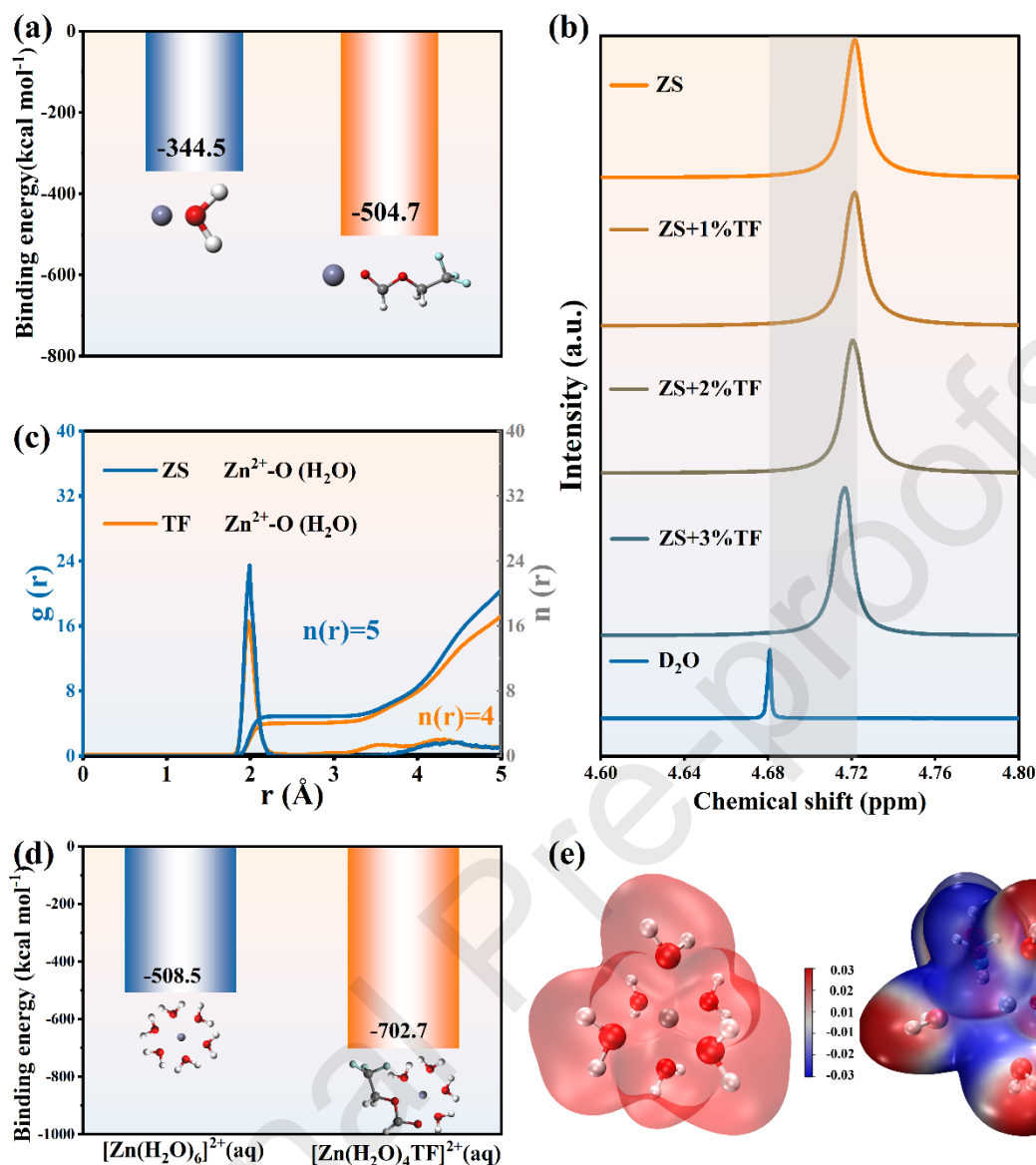
Fig. 5 (a) Binding energies of Zn^{2+} with different compounds (left: H_2O, right: TF). (b)

NMR of ^{1}H of electrolytes with different TF concentrations. (c) RDFs of Zn^{2+}-O (H_2O)

collected in ZS and TF electrolytes. (d) Zn^{2+} solvation energies before and after the

addition of TF. (e) ESP diagrams of solventized structures of (left) pristine Zn^{2+}-$6H_2O$

and (right) TF-Zn^{2+}-$4H_2O$.

Through a combination of theoretical calculations and experimental characterizations,

the mechanism by which the TF additive inhibits the growth of Zn dendrites and side

reactions is investigated. The interactions between Zn^{2+} and H_2O or TF are studied via

22

378   quantum chemical calculations. The binding energy between Zn^{2+} and water molecules

379   (-344.5 kcal mol^{-1}) is much lower than that between Zn^{2+} and TF molecules (-504.7

380   kcal mol^{-1}), as shown in Fig. 5a, suggesting that the TF can replace water in the hydrated

381   Zn^{2+} solvated shell structure to form a new solvated structure. Nuclear magnetic

382   resonance (NMR) and Fourier transform infrared (FT-IR) spectroscopy are used to

383   study the effects of TF on the solvated structure of the hydrated Zn ions in the ZS

384   electrolytes. As shown in Fig. 5b, the ^2H peak of pure D_2O is observed at 4.6808 ppm,

385   shifting to 4.7222 ppm after the addition of 2 M $ZnSO_4$. The shift indicates that a

386   reduction in the amount of free D_2O due to the formation of a strong bond between Zn^{2+}

387   ions and the oxygen atoms of D_2O. Upon the further addition of different concentrations

388   of TF (1 %, 2 % and 3 %) to the ZS electrolytes, the ^2H peak of D_2O shifts to 4.7216,

389   4.7207 and 4.7167 ppm, respectively, indicating that the TF molecules replace part of

390   D_2O within the solvation structure of hydrated Zn^{2+}, leading to the liberation of free

391   D_2O. Furthermore, FT-IR experiments show that the addition of TF regulates the

392   structure of the solvation shell of hydrated Zn^{2+}, as shown in Fig. S17. In Fig. S17a, as

393   the TF content increases, the stretching vibration of water molecules blueshifts,

394   indicating an increase of H_2O in the electrolytic solution. On the other hand, the O-H

395   stretched vibrational band of the electrolyte water shifts to a higher wavenumber with

396   the increasing TF content as shown in Fig. S17b. This shift is attributed to the

397   weakening of the hydrophilic bonds between water molecules. The amount of Zn^{2+}-O

398   (H_2O) bonds can be obtained by radial distribution functions (RDFs) calculations as

399   shown in Figs. 5c, which determine the amount of water molecules capable of forming

400 solvation structures with Zn^{2+}. As shown in Fig. 5c, there are six H_2O around Zn^{2+} in

401 the ZS electrolyte to produce the hydrated Zn ions with Zn^{2+}. In contrast, there is a

402 reduction in Zn^{2+}-O (H_2O) in the 2 % TF electrolyte, as shown in Fig. 5c. This occurs

403 because TF infiltrates the solvated sheath layer of hydrated Zn ions and substitutes some

404 water molecules in the zinc hydrate, changing the primary solvation of the zinc hydrate.

405 In the ZS electrolyte, the $[Zn(H_2O)_6]^{2+}$ ions undergo a desolvation process near the Zn

406 anode surface when subjected to an electric field, releasing a Zn ion and six highly

407 reactive H_2O molecules. These highly chemically active H_2O tend to break down into

408 H^+ and OH^-, leading to the evolution of hydrogen and the production of the secondary

409 product ZSH. However, the entry of TF into the solvated structure of $[Zn(H_2O)_6]^{2+}$

410 reduces the presence of highly reactive H_2O, thereby preventing the formation of

411 hydrogen and byproducts. It can be seen from Fig. 5d that the desolvation energies of

412 Zn^{2+} and H_2O before and after the addition of TF are -508.5 kcal mol^{-1} and -702.7 kcal

413 mol^{-1}, respectively. This implies that the addition of TF changes the structure of the

414 Zn^{2+} solution and reduces the amount of active H_2O. In addition, the introduction of a

415 TF molecule to replace two H_2O molecules in the original solvated structure

416 $[Zn(H_2O)_6]^{2+}$ leads to a significant reduction in the electrostatic potential value (Fig.

417 5e), indicating that electric repulsive forces around the Zn ion can be alleviated,

418 facilitating rapid Zn^{2+} transport.
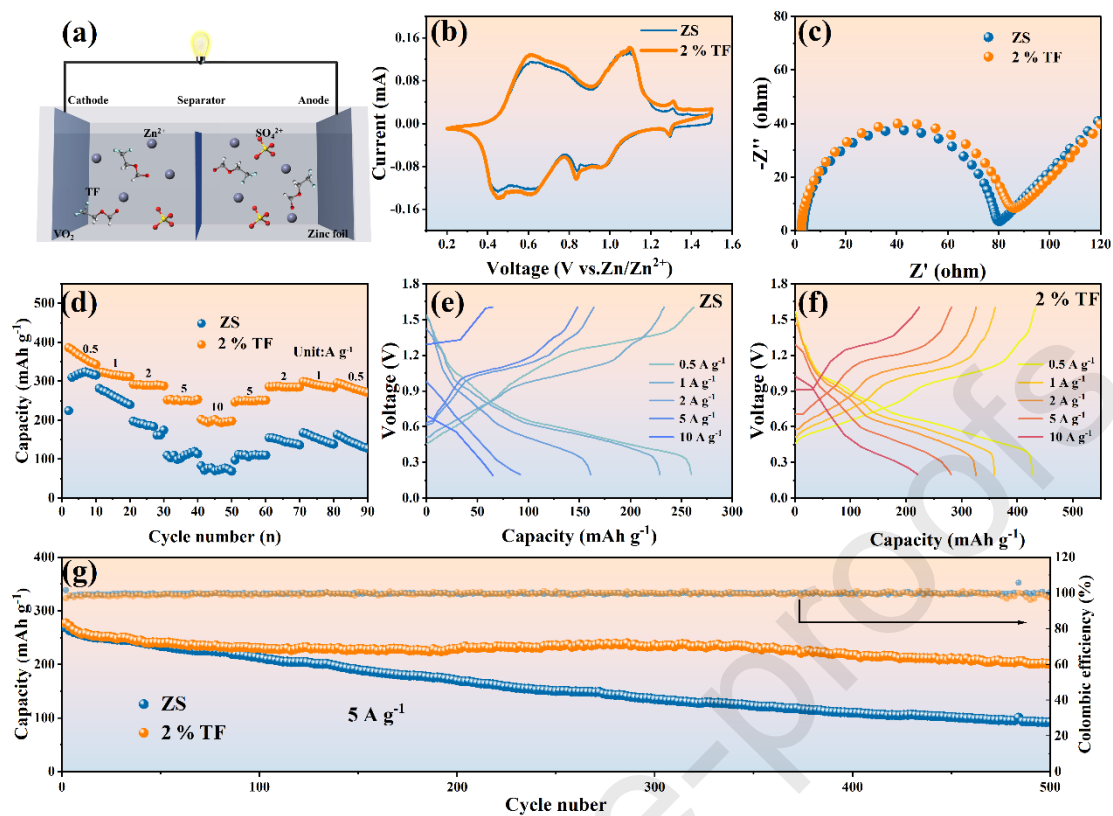
Fig. 6 (a) Schematic of $Zn//VO_2$ full cells. (b) CV curves of $Zn//VO_2$ full cell in ZS and 2 % TF electrolytes at a scan rate of 0.1 mV s^{-1}. (c) EIS plots of $Zn//VO_2$ cells assembled in ZS and 2 % TF electrolytes. (d) Rate performance of $Zn//VO_2$ full cells at current densities from 0.5 to 10 A g^{-1}. (e, f) Galvanostatic discharge/charge curves of $Zn//VO_2$ full cell in ZS and 2 % TF electrolytes at various current densities. (g) Long-term cycling of $Zn//VO_2$ full cells in ZS and 2 % TF electrolytes at 5 A g^{-1}.

To demonstrate the practicality of the 2 % TF electrolyte, we use VO_2 as the cathode and Zn metal as the anode with either ZS or 2 % TF electrolytes to assemble a full battery. The schematic of the full battery is shown in Fig. 6a. The XRD pattern and SEM image of VO_2 are shown in Fig. S18, indicating the success of VO_2 synthesis. The peaks observed at 5 – 10° correspond to $V_5O_{12}\cdot 6H_2O$ and V_6O_{13}, indicating incomplete reduction of vanadium during the hydrothermal process (Fig. S19). The CV curves of

25

432   Zn//VO$_2$ full cells with ZS and 2 % TF electrolytes show similar redox peaks (Fig. 6b),

433   indicating that the redox reactions of Zn and VO$_2$ are not affected by the addition of

434   TF. The EIS plots of Zn//VO$_2$ cells in the various electrolyte solutions (Fig. 6c) show

435   that the battery impedance does not change much after adding 2 % TF. As shown in

436   Figs. 6d – f, the specific capacities of Zn//VO$_2$ cell in the 2 % TF electrolyte are 362,

437   315, 290, 251, 196, 250, 284, 287 and 288 mAh g^{-1} at current densities of 0.5, 1, 2, 5,

438   10, 5, 2, 1 and 0.5 A g^{-1}, respectively, which are much higher than that of cell in the ZS

439   electrolyte. Long-term cycle behaviors of Zn//VO$_2$ cells before and after the addition

440   of TF at 5 A g^{-1} is shown in Fig. 5g. The full cell with the addition of TF exhibits a

441   superior performance with a capacity retention of 72.5 % after 500 cycles, significantly

442   better than that in the ZS electrolyte (34.4 %). Surprisingly, even at a small current

443   density of 0.5 A g^{-1}, a full battery cycled in the 2 % TF electrolyte exhibits superior

444   capacity retention rate (Fig. S20). Fig. S21 presents the SEM images of Zn anodes of

445   Zn//VO$_2$ full batteries cycled for 100 cycles, with and without the addition of TF. A

446   dendritic cluster surface is observed on the anode in the ZS electrolyte, indicating strong

447   dendritic growth and side reactions during the electrochemical reaction. In contrast, the

448   Zn anodes of the full cell in the 2 % TF electrolyte exhibit a smooth, flat, and dense

449   surface after 100 cycles. The morphology of VO$_2$ cathode material after cycling in the

450   TF electrolyte exhibits significant improvement compared to that observed after cycling

451   in ZS electrolyte (Figs. S21c, d).

452

453

4. Conclusion

To inhibit the formation of zinc (Zn) dendrites and by-products on Zn anodes during electrochemical reactions, simple organic TF molecules have been developed as a highly efficient electrolyte additive for aqueous zinc-ion batteries (AZIBs). Owing to strong binding energies associated with Zn^{2+}, 2,2,2-trifluoroether formate (TF) enables infiltration into the solvated sheath of hydrated Zn^{2+} and reduce the amount of highly reactive H_2O. Simultaneously, the TF molecules can be preferably adsorbed on the surface of Zn metal, facilitating the uniform deposition of Zn^{2+} along the crystalline surface of Zn (002). Accordingly, the asymmetric Zn//Cu battery with 2 % TF electrolyte allows for stable cycling for over 3,800 cycles at 2 mA cm^{-2} with the average Columbic efficiency (CE) of 99.81 %. The Zn||Zn-symmetric batteries incorporated 2 % TF demonstrate a long cycle life, exceeding 3,800 and 2,400 hours at 2 mA cm^{-2} and 5 mA cm^{-2}, respectively. The addition of TF significantly prolongs the cycle life of the Zn||Zn-symmetric batteries, showing comparable or even superior cycle life and cumulative capacity to recently reported work on electrolyte additives[54, 61]. Meanwhile, the Zn//VO_2 cells with 2 % TF exhibit the high initial capacity of 276.8 mAh g^{-1} and capacity retention rate of 72.5 % at 5 A g^{-1} after 500 cycles. This work provides a comprehensive electrolyte design strategy aimed at suppressing Zn dendrite growth and minimizing side reactions, thereby enabling the realization of long-lasting Zn metal anodes in AZIBs.

481 LTD (www.kexingtest.com) for the SEM tests.

482

Notes

484 The authors declare no competing financial interest.

485

References

487 [1] H. Yang, D. Chen, R. Zhao, G. Li, H. Xu, L. Li, X. Liu, G. Li, D. Chao, W. Han,

488 Reunderstanding aqueous Zn electrochemistry from interfacial specific adsorption of solvation

489 structures, Energy & Environmental Science 16(7) (2023) 2910-2923.

490 https://doi.org/10.1039/d3ee00658a.

491 [2] X. Yu, Z. Li, X. Wu, H. Zhang, Q. Zhao, H. Liang, H. Wang, D. Chao, F. Wang, Y. Qiao, H.

492 Zhou, S.-G. Sun, Ten concerns of Zn metal anode for rechargeable aqueous zinc batteries,

493 Joule 7(6) (2023) 1145-1175. https://doi.org/10.1016/j.joule.2023.05.004.

494 [3] Y. Chen, Q. Li, P. Wang, X. Liao, J. Chen, X. Zhang, Q. Zheng, D. Lin, K.h. Lam, High-

495 Energy-Density Cathode Achieved via the Activation of a Three-Electron Reaction in Sodium

496 Manganese Vanadium Phosphate for Sodium-Ion Batteries, Small 19(50) (2023) 2304002.

497 https://doi.org/10.1002/smll.202304002.

498 [4] X. Shi, Z. Xu, Y. Tang, Y. Zhao, B. Lu, J. Zhou, Nitrogen/phosphorus co-doped carbon

499 decorated with metallic zinc for high-performance potassium-ion batteries, Applied Physics

500 Letters 123(4) (2023). https://doi.org/10.1063/5.0161658.

501 [5] T. Wang, Y. Zhang, J. You, F. Hu, Recent Progress in Aqueous Zinc-Ion Batteries: From

502 FundamentalScience to Structure Design, The Chemical Record 23(5) (2023).

503   https://doi.org/10.1002/tcr.202200309.

504   [6] J. Yang, B. Yin, Y. Sun, H. Pan, W. Sun, B. Jia, S. Zhang, T. Ma, Zinc Anode for Mild

505   Aqueous Zinc-Ion Batteries: Challenges, Strategies, and Perspectives, Nano-Micro Letters

506   14(1-47) (2022). https://doi.org/10.1007/s40820-021-00782-5.

507   [7] Y. Chen, X. Liao, P. Wang, J. Chen, X. Zhang, X. Wu, S.C. Smith, D. Lin, X. Tan, Q.

508   Zheng, A high-energy-density NASICON-type Na3V1.25Ga0.75(PO4)3 cathode with

509   reversible V4+/V5+ redox couple for sodium ion batteries, Journal of Colloid and Interface

510   Science 653 (2024) 1-10. https://doi.org/10.1016/j.jcis.2023.09.057.

511   [8] C. Nie, G. Wang, D. Wang, M. Wang, X. Gao, Z. Bai, N. Wang, J. Yang, Z. Xing, S. Dou,

512   Recent Progress on Zn Anodes for Advanced Aqueous Zinc-Ion Batteries, Advanced Energy

513   Materials 13(28) (2023). https://doi.org/10.1002/aenm.202300606.

514   [9] L. Yuan, J. Hao, C.-C. Kao, C. Wu, H.-K. Liu, S.-X. Dou, S.-Z. Qiao, Regulation methods

515   for the Zn/electrolyte interphase and the effectiveness evaluation in aqueous Zn-ion batteries,

516   Energy & Environmental Science 14(11) (2021) 5669-5689.

517   https://doi.org/10.1039/d1ee02021h.

518   [10] H. Cao, X. Zhang, B. Xie, X. Huang, F. Xie, Y. Huo, Q. Zheng, R. Zhao, Q. Hu, L. Kang,

519   S. Liu, D. Lin, Unraveling the Solvation Structure and Electrolyte Interface through Carbonyl

520   Chemistry for Durable and Dendrite-Free Zn anode, Advanced Functional Materials 33(46)

521   (2023) 2305638. https://doi.org/10.1002/adfm.202305683.

522   [11] X. Zhang, J. Chen, H. Cao, X. Huang, Y. Liu, Y. Chen, Y. Huo, D. Lin, Q. Zheng, K.h.

523   Lam, Efficient Suppression of Dendrites and Side Reactions by Strong Electrostatic Shielding

524   Effect via the Additive of Rb2SO4 for Anodes in Aqueous Zinc-Ion Batteries, Small 19(52)

525 (2023) 2303906. https://doi.org/10.1002/smll.202303906.

526 [12] J. Chen, L. Su, X. Zhang, Y. Chen, P. Wang, Q. Zheng, D. Lin, Ethylene Glycol

527 Intercalation Engineered Interplanar Spacing and Redox Activity of Ammonium Vanadate

528 Nanoflowers as a High-Performance Cathode for Aqueous Zinc–Ion Batteries, ACS

529 Sustainable Chemistry & Engineering 11(33) (2023) 12467-12476.

530 https://doi.org/10.1021/acssuschemeng.3c03386.

531 [13] H. Li, S. Guo, H. Zhou, Recent advances in manipulating strategy of aqueous electrolytes

532 for Zn anode stabilization, Energy Storage Materials 56 (2023) 227-257.

533 https://doi.org/10.1016/j.ensm.2023.01.027.

534 [14] J. Yang, R. Zhao, Y. Wang, Z. Hu, Y. Wang, A. Zhang, C. Wu, Y. Bai, Insights on

535 Artificial Interphases of Zn and Electrolyte: Protection Mechanisms, Constructing Techniques,

536 Applicability, and Prospective, Advanced Functional Materials 33(14) (2023) 2213510.

537 https://doi.org/10.1002/adfm.202213510.

538 [15] X. Li, Z. Chen, P. Ruan, X. Hu, B. Lu, X. Yuan, S. Tian, J. Zhou, Inducing preferential

539 growth of the Zn (002) plane by using a multifunctional chelator for achieving highly reversible

540 Zn anodes, Nanoscale 16(6) (2024) 2923-2930. https://doi.org/10.1039/d3nr05699f.

541 [16] J. Li, Z. Liu, S. Han, P. Zhou, B. Lu, J. Zhou, Z. Zeng, Z. Chen, J. Zhou, Hetero Nucleus

542 Growth Stabilizing Zinc Anode for High-Biosecurity Zinc-Ion Batteries, Nano-Micro Letters

543 15(1) (2023). https://doi.org/10.1007/s40820-023-01206-2.

544 [17] W. Yang, Y. Yang, H. Yang, H. Zhou, Regulating Water Activity for Rechargeable Zinc-

545 Ion Batteries: Progress and Perspective, ACS Energy Letters 7(8) (2022) 2515-2530.

546 https://doi.org/10.1021/acsenergylett.2c01152.

547   [18] X. Zhang, J.P. Hu, N. Fu, W.B. Zhou, B. Liu, Q. Deng, X.W. Wu, Comprehensive review

548   on zinc-ion battery anode: Challenges and strategies, InfoMat 4(7) (2022) e12306.

549   https://doi.org/10.1002/inf2.12306.

550   [19] M. Peng, X. Tang, K. Xiao, T. Hu, K. Yuan, Y. Chen, Polycation-Regulated Electrolyte

551   and Interfacial Electric Fields for Stable Zinc Metal Batteries, Angewandte Chemie

552   International Edition 62(27) (2023) e202302701. https://doi.org/10.1002/anie.202302701.

553   [20] Y. Liang, M. Qiu, P. Sun, W. Mai, Comprehensive Review of Electrolyte Modification

554   Strategies for Stabilizing Zn Metal Anodes, Advanced Functional Materials 33(51) (2023)

555   2304878. https://doi.org/10.1002/adfm.202304878.

556   [21] B. Liu, X. Yuan, Y. Li, Colossal Capacity Loss during Calendar Aging of Zn Battery

557   Chemistries, ACS Energy Letters 8(9) (2023) 3820-3828.

558   https://doi.org/10.1021/acsenergylett.3c01282.

559   [22] Z. Zhang, Y. Zhang, M. Ye, Z. Wen, Y. Tang, X. Liu, C.C. Li, Lithium Bis(oxalate)borate

560   Additive for Self-repairing Zincophilic Solid Electrolyte Interphases towards Ultrahigh-rate and

561   Ultra-stable Zinc Anodes, Angewandte Chemie International Edition 62 (2023) e202311032.

562   https://doi.org/10.1002/anie.202311032.

563   [23] H. Li, R. Zhao, W. Zhou, L. Wang, W. Li, D. Zhao, D. Chao, Trade-off between

564   Zincophilicity and Zincophobicity: Toward Stable Zn-Based Aqueous Batteries, JACS Au 3(8)

565   (2023) 2107-2116. https://doi.org/10.1021/jacsau.3c00292.

566   [24] Y.F. Tian, S.J. Tan, Z.Y. Lu, D.X. Xu, H.X. Chen, C.H. Zhang, X.S. Zhang, G. Li, Y.M.

567   Zhao, W.P. Chen, Q. Xu, R. Wen, J. Zhang, Y.G. Guo, Insights into Anion-Solvent

568   Interactions to Boost Stable Operation of Ether-Based Electrolytes in Pure-

569   SiOx||LiNi0.8Mn0.1Co0.1O2 Full Cells, Angewandte Chemie International Edition 62(33)

570   (2023) e202305988. https://doi.org/10.1002/anie.202305988.

571   [25] H. Yu, D. Chen, T. Zhang, M. Fu, J. Cai, W. Wei, X. Ji, Y. Chen, L. Chen, Insight on the

572   Double-Edged Sword Role of Water Molecules in the Anode of Aqueous Zinc-Ion Batteries,

573   Small Structures 3(12) (2022). https://doi.org/10.1002/sstr.202200143.

574   [26] H. Yu, C. Lv, C. Yan, G. Yu, Interface Engineering for Aqueous Aluminum Metal

575   Batteries: Current Progresses and Future Prospects, Small Methods (2023).

576   https://doi.org/10.1002/smtd.202300758.

577   [27] F. Wu, Y. Chen, Y. Chen, R. Yin, Y. Feng, D. Zheng, X. Xu, W. Shi, W. Liu, X. Cao,

578   Achieving Highly Reversible Zinc Anodes via N, N-Dimethylacetamide Enabled Zn-Ion

579   Solvation Regulation, Small 18(27) (2022) 2202363. https://doi.org/10.1002/smll.202202363.

580   [28] J. Luo, L. Xu, Y. Zhou, T. Yan, Y. Shao, D. Yang, L. Zhang, Z. Xia, T. Wang, L. Zhang, T.

581   Cheng, Y. Shao, Regulating the Inner Helmholtz Plane with a High Donor Additive for Efficient

582   Anode Reversibility in Aqueous Zn-Ion Batteries, Angewandte Chemie International Edition

583   62(21) (2023) e202302302. https://doi.org/10.1002/anie.202302302.

584   [29] J. Li, S. Zhou, Y. Chen, X. Meng, A. Azizi, Q. He, H. Li, L. Chen, C. Han, A. Pan, Self-

585   Smoothing Deposition Behavior Enabled by Beneficial Potential Compensating for Highly

586   Reversible Zn-Metal Anodes, Advanced Functional Materials (2023) 2307201.

587   https://doi.org/10.1002/adfm.202307201.

588   [30] C. You, R. Wu, X. Yuan, L. Liu, J. Ye, L. Fu, P. Han, Y. Wu, An inexpensive electrolyte

589   with double-site hydrogen bonding and a regulated Zn2+ solvation structure for aqueous Zn-

590   ion batteries capable of high-rate and ultra-long low-temperature operation, Energy &

591   Environmental Science 16(11) (2023) 5096-5107. https://doi.org/10.1039/d3ee01741a.

592   [31] R. Wang, Q. Ma, L. Zhang, Z. Liu, J. Wan, J. Mao, H. Li, S. Zhang, J. Hao, L. Zhang, C.

593   Zhang, An Aqueous Electrolyte Regulator for Highly Stable Zinc Anode Under −35 to 65 °C,

594   Advanced Energy Materials 13(40) (2023) 2302543.

595   https://doi.org/10.1002/aenm.202302543.

596   [32] L. Liu, H. Lu, C. Han, X. Chen, S. Liu, J. Zhang, X. Chen, X. Wang, R. Wang, J. Xu, H.K.

597   Liu, S.X. Dou, W. Li, Salt Anion Amphiphilicity-Activated Electrolyte Cosolvent Selection

598   Strategy toward Durable Zn Metal Anode, ACS Nano 17(22) (2023) 23065-23078.

599   https://doi.org/10.1021/acsnano.3c08716.

600   [33] T. Lu, F. Chen, Multiwfn: A multifunctional wavefunction analyzer, Journal of

601   Computational Chemistry 33(5) (2012) 580-592. https://doi.org/10.1002/jcc.22885.

602   [34] A.D. W. Humphrey, K. Schulten, VMD: Visual Molecular Dynamics, J Mol Graph 14

603   (1996) 33.

604   [35] M.T.C. R. F. W. Bader, J. R. Cheeseman, C. Chang,, Properties of Atoms in Molecules:

605   Atomic Volumes, J. Am. Chem. Soc 109 (1987) 7968.

606   [36] M. Zhou, S. Guo, J. Li, X. Luo, Z. Liu, T. Zhang, X. Cao, M. Long, B. Lu, A. Pan, G. Fang,

607   J. Zhou, S. Liang, Surface-Preferred Crystal Plane for a Stable and Reversible Zinc Anode,

608   Advanced Materials 33(21) (2021) 2100187. https://doi.org/10.1002/adma.202100187.

609   [37] T.C. Li, C. Lin, M. Luo, P. Wang, D.-S. Li, S. Li, J. Zhou, H.Y. Yang, Interfacial Molecule

610   Engineering for Reversible Zn Electrochemistry, ACS Energy Letters 8(8) (2023) 3258-3268.

611   https://doi.org/10.1021/acsenergylett.3c00859.

612   [38] Y. Wang, L.e. Mo, X. Zhang, Y. Ren, T. Wei, Z. Li, Y. Huang, H. Zhang, G. Cao, L. Hu,

613   Facet-Termination Promoted Uniform Zn (100) Deposition for High-Stable Zinc-Ion Batteries,

614   Advanced Energy Materials 13(31) (2023) 2301517.

615   https://doi.org/10.1002/aenm.202301517.

616   [39] Y. Lin, Z. Mai, H. Liang, Y. Li, G. Yang, C. Wang, Dendrite-free Zn anode enabled by

617   anionic surfactant-induced horizontal growth for highly-stable aqueous Zn-ion pouch cells,

618   Energy & Environmental Science 16(2) (2023) 687-697. https://doi.org/10.1039/d2ee03528f.

619   [40] J. Wan, R. Wang, Z. Liu, L. Zhang, F. Liang, T. Zhou, S. Zhang, L. Zhang, Q. Lu, C.

620   Zhang, Z. Guo, A Double-Functional Additive Containing Nucleophilic Groups for High-

621   Performance Zn-Ion Batteries, ACS Nano 17(2) (2023) 1610-1621.

622   https://doi.org/10.1021/acsnano.2c11357.

623   [41] G. Ma, L. Miao, Y. Dong, W. Yuan, X. Nie, S. Di, Y. Wang, L. Wang, N. Zhang,

624   Reshaping the electrolyte structure and interface chemistry for stable aqueous zinc batteries,

625   Energy Storage Materials 47 (2022) 203-210. https://doi.org/10.1016/j.ensm.2022.02.019.

626   [42] Z. Liu, R. Wang, Q. Ma, J. Wan, S. Zhang, L. Zhang, H. Li, Q. Luo, J. Wu, T. Zhou, J.

627   Mao, L. Zhang, C. Zhang, Z. Guo, A Dual-Functional Organic Electrolyte Additive with

628   Regulating Suitable Overpotential for Building Highly Reversible Aqueous Zinc Ion Batteries,

629   Advanced Functional Materials 34(5) (2023) 2214538.

630   https://doi.org/10.1002/adfm.202214538.

631   [43] H. Yu, D. Chen, Q. Li, C. Yan, Z. Jiang, L. Zhou, W. Wei, J. Ma, X. Ji, Y. Chen, L. Chen,

632   In Situ Construction of Anode–Molecule Interface via Lone-Pair Electrons in Trace Organic

633   Molecules Additives to Achieve Stable Zinc Metal Anodes, Advanced Energy Materials 13(22)

634   (2023) 2300550. https://doi.org/10.1002/aenm.202300550.

635   [44] M. Kim, S.J. Shin, J. Lee, Y. Park, Y. Kim, H. Kim, J.W. Choi, Cationic Additive with a

636   Rigid Solvation Shell for High-Performance Zinc Ion Batteries, Angewandte Chemie

637   International Edition 61(47) (2022) e202211589. https://doi.org/10.1002/anie.202211589.

638   [45] T. Wei, Y. Ren, Y. Wang, L. Mo, Z. Li, H. Zhang, L. Hu, G. Cao, Addition of Dioxane in

639   Electrolyte Promotes (002)-Textured Zinc Growth and Suppressed Side Reactions in Zinc-Ion

640   Batteries, ACS Nano 17(4) (2023) 3765-3775. https://doi.org/10.1021/acsnano.2c11516.

641   [46] C. Li, G. Qu, X. Zhang, C. Wang, X. Xu, Electrode/Electrolyte Interfacial Chemistry

642   Modulated by Chelating Effect for High-Performance Zinc Anode, Energy & Environmental

643   Materials 0 (2023) e12608. https://doi.org/10.1002/eem2.12608.

644   [47] F. Yang, J.A. Yuwono, J. Hao, J. Long, L. Yuan, Y. Wang, S. Liu, Y. Fan, S. Zhao, K.

645   Davey, Z. Guo, Understanding H(2) Evolution Electrochemistry to Minimize Solvated Water

646   Impact on Zinc-Anode Performance, Adv Mater 34(45) (2022) e2206754.

647   https://doi.org/10.1002/adma.202206754.

648   [48] Y. Lyu, J.A. Yuwono, P. Wang, Y. Wang, F. Yang, S. Liu, S. Zhang, B. Wang, K. Davey,

649   J. Mao, Z. Guo, Organic pH Buffer for Dendrite-Free and Shuttle-Free Zn-I2 Batteries,

650   Angewandte Chemie International Edition 62(21) (2023) e202303011.

651   https://doi.org/10.1002/anie.202303011.

652   [49] N. Wang, X. Chen, H. Wan, B. Zhang, K. Guan, J. Yao, J. Ji, J. Li, Y. Gan, L. Lv, L. Tao,

653   G. Ma, H. Wang, J. Zhang, H. Wang, Zincophobic Electrolyte Achieves Highly Reversible Zinc

654   -Ion Batteries, Advanced Functional Materials 33(27) (2023) 2300795.

655   https://doi.org/10.1002/adfm.202300795.

656   [50] B. Niu, Z. Li, D. Luo, X. Ma, Q. Yang, Y.-E. Liu, X. Yu, X. He, Y. Qiao, X. Wang, Nano-

657 scaled hydrophobic confinement of aqueous electrolyte by a nonionic amphiphilic polymer for

658 long-lasting and wide-temperature Zn-based energy storage, Energy & Environmental

659 Science 16(4) (2023) 1662-1675. https://doi.org/10.1039/d2ee04023a.

660 [51] T. Zhang, J. Yang, H. Wang, H. Yu, Q. Li, L. Chen, Y. Chen, T. Wang, A solubility-limited,

661 non-protonic polar small molecule co-solvent reveals additive selection in inorganic zinc salts,

662 Energy Storage Materials 65 (2024). https://doi.org/10.1016/j.ensm.2023.103085.

663 [52] H. Yu , D. Chen , X. Ni, P. Qing, C. Yan, W. Wei, J. Ma, X. Ji, Y. Chen, L. Chen,

664 Reversible Adsorption with Oriented Arrangement of Zwitterionic Additive Stabilizes

665 Electrodes for Ultralong-Life Zn-Ion Batteries, Energy Environ. Sci. 16 (2023) 2684-2695.

666 https://doi.org/10.1039/D3EE00982C.

667 [53] Z. Wang, J. Diao, J.N. Burrow, K.K. Reimund, N. Katyal, G. Henkelman, C.B. Mullins,

668 Urea-Modified Ternary Aqueous Electrolyte With Tuned Intermolecular Interactions and

669 Confined Water Activity for High-Stability and High-Voltage Zinc-Ion Batteries, Advanced

670 Functional Materials 33(48) (2023) 2304791. https://doi.org/10.1002/adfm.202304791.

671 [54] M. Kim, J. Lee, Y. Kim, Y. Park, H. Kim, J.W. Choi, Surface Overpotential as a Key Metric

672 for the Discharge-Charge Reversibility of Aqueous Zinc-Ion Batteries, J Am Chem Soc

673 145(29) (2023) 15776-15787. https://doi.org/10.1021/jacs.3c01614.

674 [55] R. Chen, W. Zhang, Q. Huang, C. Guan, W. Zong, Y. Dai, Z. Du, Z. Zhang, J. Li, F. Guo,

675 X. Gao, H. Dong, J. Zhu, X. Wang, G. He, Trace Amounts of Triple-Functional Additives

676 Enable Reversible Aqueous Zinc-Ion Batteries from a Comprehensive Perspective,

677 Nanomicro Lett 15(1) (2023) 81. https://doi.org/10.1007/s40820-023-01050-4.

678 [56] S. jiao, J. Fu, Q. Yin, H. Yao, H. Hu, Reconstruction of helmholtz plane to stabilize zinc

679   metal anode/electrolyte interface, Energy Storage Materials 59 (2023) 102774.

680   https://doi.org/10.1016/j.ensm.2023.102774.

681   [57] L. Zheng, H. Li, X. Wang, Z. Chen, C. Hu, K. Wang, G. Guo, S. Passerini, H. Zhang,

682   Competitive Solvation-Induced Interphases Enable Highly Reversible Zn Anodes, ACS

683   Energy Letters 8(5) (2023) 2086-2096. https://doi.org/10.1021/acsenergylett.3c00650.

684   [58] Y. Dai, C. Zhang, W. Zhang, L. Cui, C. Ye, X. Hong, J. Li, R. Chen, W. Zong, X. Gao, J.

685   Zhu, P. Jiang, Q. An, D.J.L. Brett, I.P. Parkin, G. He, L. Mai, Reversible Zn Metal Anodes

686   Enabled by Trace Amounts of Underpotential Deposition Initiators, Angew Chem Int Ed Engl

687   62(18) (2023) e202301192. https://doi.org/10.1002/anie.202301192.

688   [59] Y. Quan, M. Yang, M. Chen, W. Zhou, X. Han, J. Chen, B. Liu, S. Shi, P. Zhang,

689   Electrolyte additive of sorbitol rendering aqueous zinc-ion batteries with dendrite-free

690   behavior and good anti-freezing ability, Chemical Engineering Journal 458 (2023) 141392.

691   https://doi.org/10.1016/j.cej.2023.141392.

692   [60] H. Wang, W. Ye, B. Yin, K. Wang, M.S. Riaz, B.B. Xie, Y. Zhong, Y. Hu, Modulating

693   Cation Migration and Deposition with Xylitol Additive and Oriented Reconstruction of

694   Hydrogen Bonds for Stable Zinc Anodes, Angewandte Chemie International Edition 62(10)

695   (2023) e202218872. https://doi.org/10.1002/anie.202218872.

696   [61] H. Wang, W. Ye, B. Yin, K. Wang, M.S. Riaz, B.B. Xie, Y. Zhong, Y. Hu, Modulating

697   Cation Migration and Deposition with Xylitol Additive and Oriented Reconstruction of

698   Hydrogen Bonds for Stable Zinc Anodes, Angewandte Chemie International Edition 62(10)

699   (2023) e202218872 https://doi.org/10.1002/anie.202218872.

700